Catal Lett (2008) 125:62–68
DOI 10.1007/s10562-008-9511-8

Aluminum Containing MCF Silica as Highly Efficient Solid Acid Catalyst for Alcohol Esterification

Yong-Mei Liu · Jie Xu · Lu-Cun Wang · Yong Cao · He-Yong He · Kang-Nian Fan

Received: 17 December 2007 / Accepted: 6 May 2008 / Published online: 28 May 2008
© Springer Science+Business Media, LLC 2008

Abstract Aluminum incorporated mesocellulous silica foams (Al-MCF) with various Si/Al ratios have been hydrothermally synthesized. The characterization results indicate that the characteristic mesocellular structural features of MCF are preserved after the aluminum incorporation. The catalysts exhibit highly catalytic performance in the esterification of acetic acid with amyl alcohol in the liquid phase.

Keywords Al-MCF · Esterification · Amyl alcohol · Acidity · Hydrophobicity

1 Introduction

Organic esters are important intermediates in the synthesis of fine chemicals, drugs, plasticisers, food preservatives, pharmaceuticals, solvents, perfumes, cosmetics and chiral auxillaries [1]. Esterification is also an important reaction in synthetic organic chemistry, since it is a technique to protect carboxylic acid group in a molecule [2]. Typical catalysts for this reaction are (Brönsted acidic) sulphuric acid or (Lewis acidic) Sn-octoate [3]. Brönsted acidic homogeneous catalysts are corrosive and need to be neutralized after reaction (forming salts), whereas Lewis acidic, metal-containing, catalysts need to be removed carefully after reaction. This can be done for instance by adsorption on bleaching earth, which however leads to the formation of large amounts of waste [3].

Y.-M. Liu · J. Xu · L.-C. Wang · Y. Cao (✉) · H.-Y. He · K.-N. Fan
Department of Chemistry, Shanghai Key Laboratory of Molecular Catalysis and Innovative Materials, Fudan University, Shanghai 200433, People's Republic of China
e-mail: yongcao@fudan.edu.cn

The use of heterogeneous catalysts in esterification is preferable since they can be easily separated from reactants and products by filtration and allows the use of a continuously operated fixed bed. Many heterogeneous catalysts have been reported to be active in esterification, such as ion exchange resins, H-ZSM-5, niobic acid, sulphated oxides, and supported heteropoly acids [4]. Microporous zeolites with uniform pores have been widely used as industrial catalysts. However, they cannot catalyze reactions of large molecules due to limitation of micropore size. The discovery of mesoporous materials, such as MCM-41 has attracted much attention because of their potential use as catalyst or catalyst support for the conversion of large molecules [5]. However, as compared with conventional zeolites, these mesostructured materials have relatively low acidity and hydrothermal stability that limit their extensive use [6]. Many attempts have been made to improve the stability of MCM-41 [7] or to prepare other stable mesoporous materials [7, 8]. SBA-15, a new type of mesoporous silica with tunable pore diameter, thicker walls and much higher hydrothermal stability than MCM-41, has been prepared using tri-block copolymer as template [8]. Pure siliceous materials have electrically neutral framework and consequently no Brönsted acidity. However, it is very difficult to prepare SBA-15 containing heteroatoms in the framework because of the strong acidic synthesis conditions.

Mesocellular silica foam (MCF) is a newly reported aerogel-like mesoporous material composed of large uniform spherical cells (up to 50 nm) interconnected with uniformly sized windows featuring a continuous three-dimensional (3D) mesopore system [9]. Especially given its continuous 3D mesopore system with ultralarge pore diameters and interconnected windows, MCF materials have the advantage over their more ordered counterparts such as MCM-41 or SBA-15 of better diffusion of reactants

and products and thus overcome internal mass transfer limitations [10]. Despite of great potential use for catalytic applications, reports in literature dealing with the catalytic utilization of metal elements incorporated MCF-type materials are scarce [11]. In the present study, for the first time, a series aluminum-containing MCF catalyst was prepared and proved to be efficient solid acid catalyst for the esterification of acetic acid with amyl alcohol.

2 Experimental

2.1 Samples Preparation

The synthesis of Al-MCF using the pH adjusting method was carried out as follows: 2 g of triblock copolymer P_{123} ($EO_{20}PO_{70}EO_{20}$) was dissolved in 75 mL of HCl solution (pH = 1.5) with 1 g 1,3,5-trimethylbenzene (TMB) was stirred at 40 °C for 4 h, followed by the addition a requisite amount of Al $(NO_3)_3 \cdot 9H_2O$ to get solution A. Then, 4.25 g of TEOS and a certain amount of Al(i-PrO)3 were added to 5 mL of HCl aqueous solution at pH = 1.5 to obtain solution B, which was stirred at room temperature for about 0.5–3 h then combined with solution A. The resultant solution mixture was stirred vigorously for 20 h at 40 °C. After that, a small amount of $NH_3 \cdot H_2O$ was added drop by drop to adjust the pH value equal to 7.0. Then it was transferred into an autoclave to age for 24 h at 100 °C. The final solid was collected by filtration and dried at 100 °C. The surfactants were removed through calcination. The samples are designated as Al-MCF(*X*), where *X* stands for the Si/Al ratios in the initial gels. For comparison, Al-SBA-15 and Al-MCM-41 with similar ratio of Si/Al about 80 have been prepared following the same procedure described above.

2.2 Samples Characterization

Small-angle X-ray scattering (SAXS) experiments were performed on a Germany Bruker NanoSTAR U SAXS system equipped with high-resolution pinhole chamber using Cu $K\alpha$ radiation and 106 cm sample to detector distance. The specific surface areas were measured by N_2 adsorption using a Micromeritics TriStar 3000 equipment. The BJH method was used to determine the pore size distribution (PSD). Transmission electron microscopy (TEM) was recorded digitally on a JEOL 2011 electron microscope operating at 200 kV. FT-IR spectra were collected on a Bruker Vector 22 spectrometer using KBr pellet technique. About 10 mg of the sample was ground with about 200 mg of spectral grade KBr to form a pellet under hydraulic pressure to record the IR spectrum in the range 400–4000 cm^{-1}. In order to characterize the acidity of the catalysts, spectra of chemisorbed pyridine were monitored using self-supporting wafers in a heatable IR gas cell [10].

2.3 Activity Test

The esterification of amyl alcohol with acetic acid (or oleic acid under otherwise identical conditions) was used as a model reaction to test the catalytic activity. The reaction was performed at atmospheric pressure and refluxed in three-neck flask equipment with condenser and water separator, heated by a controlled oil batch. The molar ratio of acid: amyl alcohol was 1:2, and the weight of the catalyst used was 3 wt.% of acid. When the reactant system was heated to the reaction temperature, the catalyst was added into the system. After completion of the reactions (followed by measuring the acid consumption), the mixture was filtered. The liquid products were analyzed by a Shimadzu gas chromatograph GC-17A using a DB-5 capillary column with FID detector.

3 Results and Discussion

3.1 Structure of the Al-MCF Materials

The as-prepared Al-MCF samples have been analyzed using SAXS. X-ray scattering is observed if uniformly sized particles are present, as opposed to X-ray diffraction associated with periodic structures [12]. Figure 1A shows the recorded SAXS data for the Al-MCF samples (Si/Al = 10 in the initial gel) samples prepared with $Al(NO_3)_3 \cdot 9H_2O$ (denoted as A_1) or Al(i-PrO)$_3$ (A_2) as aluminum precursors. For the sample prepared with the mixture of $Al(NO3)_3 \cdot 9H_2O$ and Al(i-PrO)3 as aluminum precursors exhibits one strong primary peak and two higher-order peaks with exponentially decreasing intensities. The occurrence of the higher order peaks is an indication of the narrow size distribution of the spherical cells. But for the samples prepared only with $Al(NO_3)_3 \cdot 9H_2O$ or Al(i-PrO)$_3$ as aluminum precursors exhibits only one strong primary peak and no the higher-order peaks. The SAXS results show that the structure order of the materials is obviously improved by using the mixture aluminum precursors. Fluoride is a catalyst for hydrolysis and polymerization of silicon species [13] and has been used in the synthesis of purely siliceous and Ti-substituted mesoporous materials [14]. Maybe the NO_3^- species has the same effect as the NH_4F, the addition of the $Al(NO_3)_3 \cdot 9H_2O$ accelerate the hydrolysis of the TEOS.

Figure 1B shows the recorded SAXS data for the Al-MCF samples (Al_1/Al_2 = 1 in the initial gel) with Si/Al ratio ranging from 80 to 6. Although the *q* value of the first strong reflection changes slightly from sample to sample, all samples exhibit one strong primary peak and two

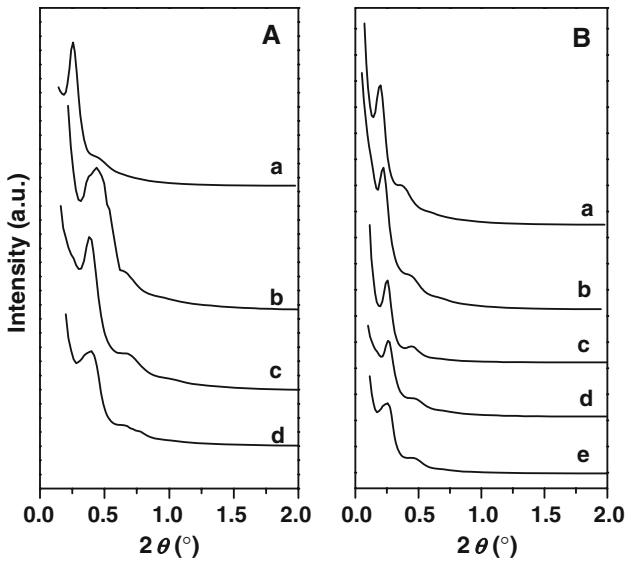

Fig. 1 Small-angle X-ray scattering patterns of calcined Al-MCF samples: **A** (a) MCF; (b) Al-MCF (10) (without Al_2); (c) Al-MCF(10) (with $Al_1/Al_2 = 1$); (d) Al-MCF (10) (without Al_1); **B** (a) Al-MCF (80) (with $Al_1/Al_2 = 1$); (b) Al-MCF (50) (with $Al_1/Al_2 = 1$) (c) Al-MCF (30) (with $Al_1/Al_2 = 1$); (d) Al-MCF (10) (with $Al_1/Al_2 = 1$); (e) Al-MCF (6) (with $Al_1/Al_2 = 1$)

higher-order peaks with exponentially decreasing intensities. The occurrence of the higher-order peaks is an indication of the narrow size distribution of the spherical cells. The sphere diameters D_s, determined from SAXS data, are given in Table 1 for Al-MCF samples with various Si/Al ratios. The D_s values agree with the cell diameters D_c, derived from nitrogen sorption, and with the cell sizes obtained from TEM (see the TEM section), and there is no decrease observed in peak intensity with the increase of Al content even if the Si/Al ratio decreases to 6. In addition, as can be seen from the diffraction patterns that the strong primary peak of calcined Al-MCF have been shifted to higher values with increasing Al content. This is consistent with previous observation reported by Borade et al. suggesting the framework substitution of Al in MCF structure [15]. This result indicates that this method allows a large amount of Al content to be incorporated while retaining its framework, as could be seen from TEM and N_2-adsorption data presented as follows.

The porosity of the Al-MCF has been investigated by N_2 sorption analyses. The isotherms are of type IV and show steep hysteresis of type H1 at high-relative pressures, which is typical for mesoporous materials that exhibit capillary condensation and evaporation and have large pore sizes with narrow size distributions. Stucky's group modification [9] of the Broekhoff-de Boer (BdB) pore size analysis makes it possible to derive the cell sizes from the adsorption branches of the isotherms, while the desorption branches give the window sizes [12]. Figure 2a shows typical isotherms and the corresponding BdB-FHH pore size analyses for sample D. The sharp peaks in the PSD plots confirm the narrow size distributions of both the cells and the windows. The BdB-FHH pore size analyses corroborate this qualitative interpretation of the isotherms (see insets in Fig. 2a and Table 1). The BET specific surface area, pore size and pore volume of all calcined samples are presented in Table 1. The BET surface areas are 400–600 m^2/g for all samples, which coincide with the reported values [12]. In particular, it can be seen that sample H presents the highest surface area and pore volume, with all pore being in the mesoporous range.

TEM image (Fig. 2b) of Al-MCF sample reveals a disordered array of silica struts comprising uniformly sized

Table 1 Characteristics of the mesostructured aluminosilicate mesocellulous foams

Samples	Al_1/Al_2 (in mol ratio)[a]	Si/Al in gel[b]	Si/Al in production[c]	BET (m^2/g)	D_s[d] (nm)	D_c[e] (nm)	D_w[e] (nm)	Volume (cm^3/g)	Terminal Si–O–[f]
A	/	∝	/	660	24.5	22.1	7.3	1.5	975
B	∝	10	15	396	22.1	17.8	5.6	1.3	905
C	0	10	14	432	22.3	17.9	7.2	1.4	902
D	1	10	13	405	24.4	22.2	5.9	1.4	897
E	1	6	8	411	24.5	22.2	6.1	1.3	897
F	1	20	26	449	24.6	22.3	6.2	1.4	907
G	1	50	58	536	30.1	27.3	6.4	1.6	950
H	1	80	91	698	31.4	29.6	7.5	1.5	966

[a] The mol ratio of Al $(NO_3)_3 \cdot 9H_2O$ to Al(i-PrO)$_3$

[b] The total mol of Al $(NO_3)_3 \cdot 9H_2O$ and Al(i-PrO)$_3$

[c] The Si/Al ratios in the calcined materials were calculated by the ICPAES method

[d] Sphere diameter, D_s, determined from SAXS analyses

[e] Cell diameter, D_C, and window diameter, D_W, determined according to the BJH method

[f] Frequencies (cm^{-1}) and suggested band assignment of the Al-MCF framework

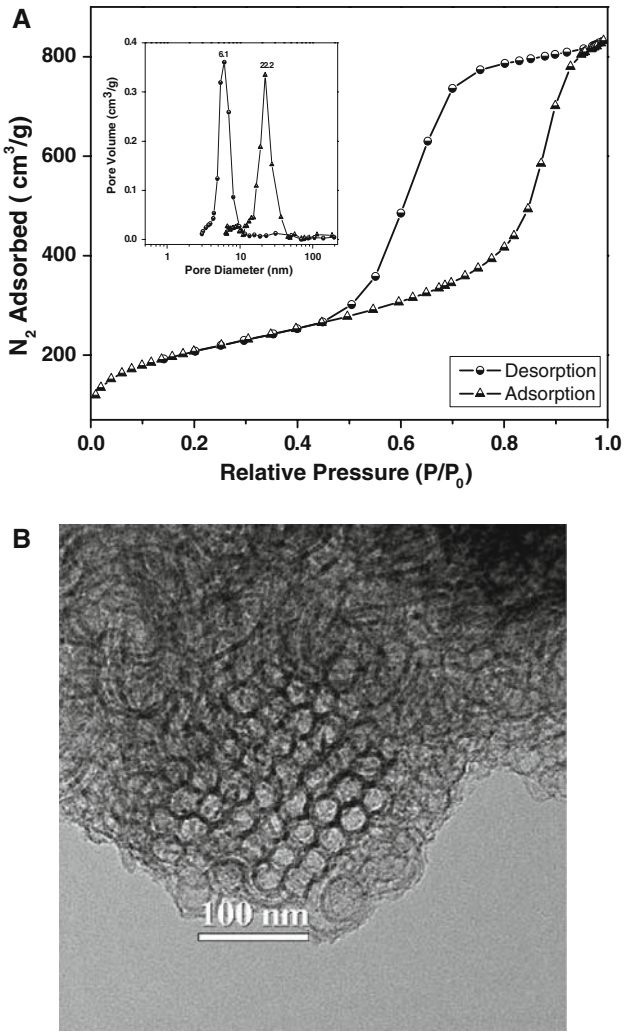

Fig. 2 (**a**) Nitrogen sorption isotherms for Al-MCF (10) (with Al_1/Al_2 = 1). Inset shows the pore size distribution (PSD) of the corresponding samples; (**b**) representative TEM image of Al-MCF(10) (with Al_1/Al_2 = 1) showing an open mesocellular structure

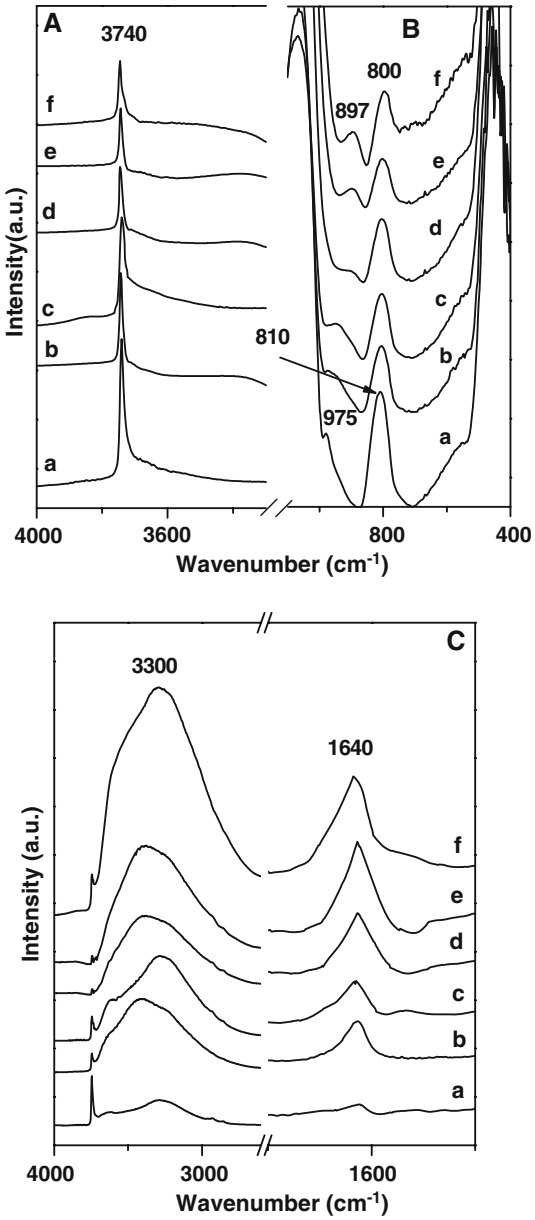

Fig. 3 FTIR spectra of the Al-MCF samples of different Si/Al ratio: (a) MCF; (b) Al-MCF (80) (with Al_1/Al_2 = 1); (c) Al-MCF (50) (with Al_1/Al_2 = 1); (d) Al-MCF (30) (with Al_1/Al_2 = 1); (e) Al-MCF (10) (with Al_1/Al_2 = 1); (f) Al-MCF (6) (with Al_1/Al_2 = 1)

spherical cells (20–34 nm) interconnected by windows with a narrow size distribution, which is the characteristic structural feature of the MCF materials [9, 12]. Note that the strut-like structure resembles that of aerogels [12]. The cell sizes estimated from TEM are consistent with the cell sizes as determined from nitrogen sorption (D_C) summarized in Table 1. The wall thickness of the Al-MCF estimated by TEM is ca. 4–6 nm, in agreement with the thick, robust framework walls observed in acid-synthesized MCF-type mesoporous silica as reported in the literature [12]. TEM analyses indicate that the continuous 3D pore structure of the MCF was robust enough to survive during the aluminum incorporation process. Slight deformations of the spherical cells can be seen in the higher magnification TEM images in Fig. 2b. Such distortions may be caused by the nonperfect packing of the spherical, colloidal particles (as discussed below) due to their slight polydispersity. The empty voids inevitably formed between nonperfectly packed spheres must be filled for energetic reasons, which may be accomplished by slight deformations of the spherical cells.

The infrared spectra of the calcined Al-MCF samples are present in Fig. 3. Figure 3A shows the spectrum of dehydrated Al-MCF samples under N_2 atmosphere in the 3800–3000 cm^{-1} range. The spectra of the pure siliceous MCF showed narrow vibration band at 3740 cm^{-1} belonging to isolated terminal silanol groups [16]. The decrease of the peak intensity attributed to the isolated terminal silanol groups with increase aluminum content

indicates that the anchoring of aluminum oxide species on to the MCF surface is accompanied by a simultaneous attenuation in the intensity of the isolated terminal silanol groups. After rehydration, the infrared spectra of the samples show an broad envelope around 3300 cm^{-1} (Fig. 3C), which is due to OH stretch of water, surface hydroxyl groups and bridged hydroxyl groups, comparison of the broad envelope due to –OH stretch of water in the higher energy region and the corresponding $–OH_2$ bending mode around 1640 cm^{-1} correlate very well with the water adsorption property (hydrophilic property) of the catalysts. The intensity of the bands due to water at the catalyst decreases in the sample order E > D > F > G > H, which is also the order of the hydrophilic property of the catalysts [17]. The peaks between 500 and 1200 cm^{-1} are assigned to framework vibrations. The intense peaks at 1038 with a shoulder at 1220 cm^{-1} are due to internal and external asymmetric Si–O stretching modes. The bands around at 810 and 449 cm^{-1} are assigned to symmetric Si–O stretching and tetrahedral Si–O bending modes, respectively, and also are slightly shifted to lower frequencies upon aluminum content samples. Such shifts in frequencies would reflect the formation of new Si–O–Si and Si–O–Al bridges during calcinations. In this way, it is probably due to an increased network cross linking [18]. In addition, the weak bands at 975 cm^{-1} are attributed to defect sites (Si–OH). Since both $Si–O^-$ and $Al–O^-$ stretching bands appear nearly in the same region (800–1100 cm^{-1}) and hence they cannot be clearly distinguished. However, a small shift toward the lower wave number (Table 1 and Fig. 3B) could be noticed for Al-MCF as compared to siliceous MCF as a result of the incorporation of Al for Si in the framework structure. All these features are typical characteristics of aluminosilicate of MCF structure [19].

To evaluate the strength and types of acid sites of Al-MCF, pyridine adsorption measured by IR spectroscopy was used. Figure 4 shows the spectra of pyridine desorbed on Al-MCF at 150 °C in the range 1700–1400 cm^{-1} for samples with different Si/Al ratios. All the samples show bands corresponding to hydrogen-bonded pyridine (1445 and 1596 cm^{-1}), Lewis acidic sites bound pyridine (1450 and 1623 cm^{-1}) and Brönsted acidic sites bound pyridine (1545 and 1640 cm^{-1}). An additional band appears at 1490 cm^{-1} attributed to pyridine associated with both Brönsted and Lewis acidic sites [20, 21]. It can be seen from figure that the increase in aluminum content lead to an increase in acidic sites, viz., Lewis and Brönsted acidic sites, which is in good agreement with the results reported by Wang et al. [23]. The intensity of the bands at 1455 and 1547 cm^{-1} due to Lewis and Brönsted acid sites increases with decreasing Si/Al ratios. This indicates that the acidity increases with increasing Al contents. The IR spectrum of pyridine adsorption on pure silica MCF material shows no peaks at

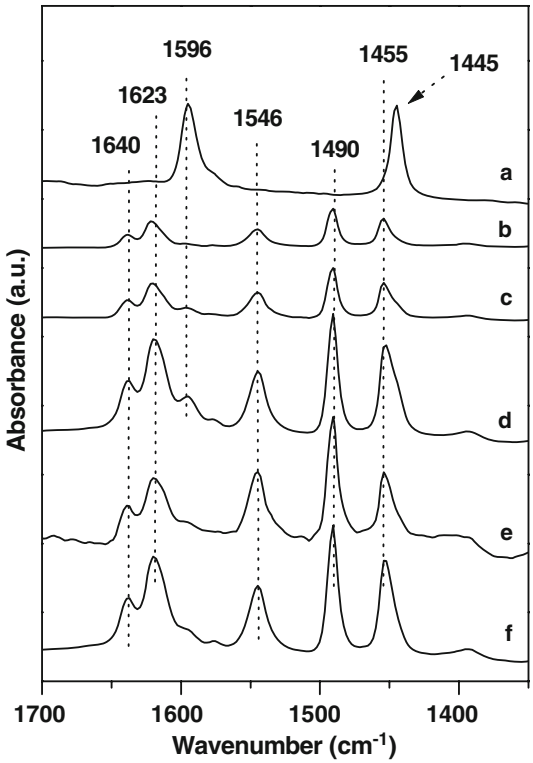

Fig. 4 IR spectra of pyridine desorbed on Al-MCF with different Si/Al ratios at 150 °C: (a) MCF; (b) Al-MCF (80) (with $Al_1/Al_2 = 1$); (c) Al-MCF(50) (with $Al_1/Al_2 = 1$); (d) Al-MCF (30) (with $Al_1/Al_2 = 1$); (e) Al-MCF (10) (with $Al_1/Al_2 = 1$); (f) Al-MCF (6) (with $Al_1/Al_2 = 1$)

1455 or 1547 cm^{-1} attributed to Lewis or Brönsted acid sites, respectively.

3.2 Catalytic Performance

The esterification of acetic acid with amyl alcohol is an electrophilic substitution. The reaction is relatively slow and needs activation either by high temperature or by a catalyst to facilitate the overall reaction [16, 20]. Figure 5 illustrates the catalytic performance of Al-MCF samples with various Si/Al ratios for the esterification of acetic acid. It is seen that higher conversion was obtained over Al-MCF with higher Si/Al ratios. Since they are more hydrophobic, once water is produced it will be easily be expelled from the pores thus avoiding the associated poisoning effect. Water acting as an adsorption poison over solid acid catalysts has also been reported in the literature [21]. These rationalizations account for the order of activity of the catalysts H > G > F > D > E. Yet another advantage for high silica materials is the hydrophobic amyl alcohol can be better delivered into the pores than those with low Si/Al ratios, which are less hydrophobic. At this juncture, it is interesting to note that the most active H sample has however the weakest surface acidity as

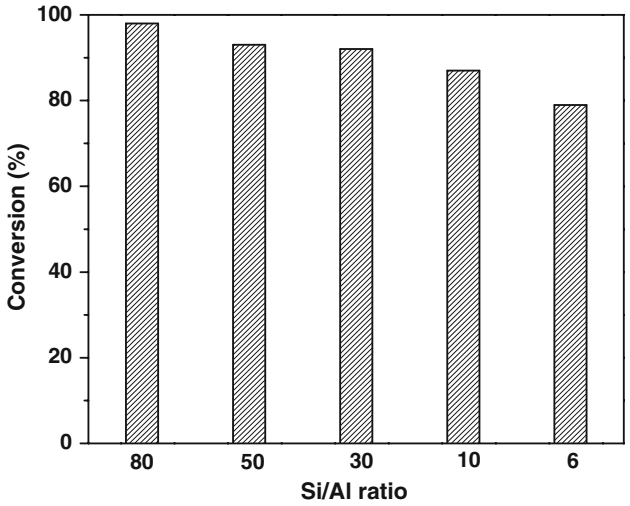

Fig. 5 The effect of Si/Al ratio on the esterification of amyl alcohol with acetic acid over Al-MCF. *Reaction conditions*: catalyst weight = 0.03 g; molar ratio = 2:1 (amyl alcohol/acetic acid); temperature = 120 °C; time = 3 h; pressure = autogenous

reflected from pyridine adsorption data, inferring that the surface hydrophobicity may play more important role in determining the catalytic behavior of the Al-MCF materials in the esterification of acetic acid with amyl alcohol.

To obtain more information regarding the possible effect of framework structure on the activity of the aluminosilicate materials, a comparative study of the esterification of acetic acid or oleic acid with amyl alcohol was tested over different catalysts with roughly the same Si/Al ratio ($\sim$ 80). As illustrated in Fig. 6, in all cases, the conversion of the acetic acid is observed to be appreciably higher than using oleic acid as the reaction substrate. It is clear that the ZSM-5 material show the lowest activity as compared to all other samples. This could be attributed to their intrinsic

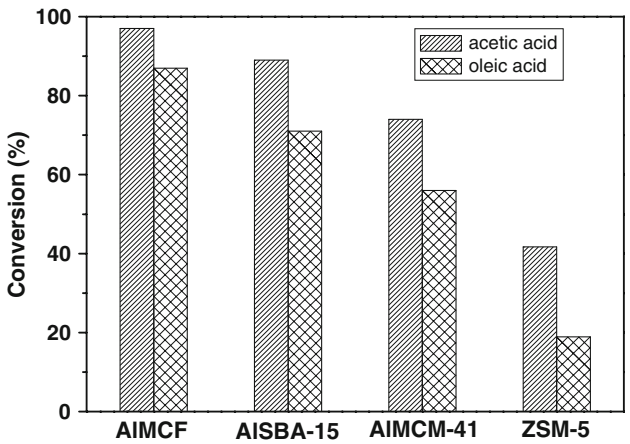

Fig. 6 A comparison of esterification of amyl alcohol with acetic acid and oleic acid over various materials. *Reaction conditions*: catalyst weight = 0.03 g; molar ratio = 2:1 (amyl alcohol/acid); temperature = 120 °C; time = 3 h; pressure = autogenous

microporous nature which may present severe mass transfer limitations in the liquid phase reactions [17]. In a comparison of three different aluminosilicate materials with a mesoporous structure, it is observed that the Al-MCF sample featured with a well-defined 3D mesoporosity with ultralarge mesopores are more effective, as demonstrated by the higher activities observed for this sample. Additionally, with a similar hexagonally arranged framework structure, Al-SBA-15 with a larger pore diameter is much superior to Al-MCM-41 as an acid catalyst. It is, therefore, concluded that the enhanced esterification activity achievable over the mesostructured Al-MCF catalysts is strongly related to the larger pore diameters and unique 3D mesoporosity which can provide more favorable conditions for mass transfer thus leading to enhanced performance for esterification reaction.

4 Conclusions

A series of mesostructured aluminosilicate MCF materials have been successfully synthesized by pH-adjusting method. Such materials showed high activity toward the esterification of acetic acid with amyl alcohol. Despite a lower surface acidity, Al-MCF(80) with more surface hydrophobicity was found to be more active than the other catalysts with lower Si/Al ratio. The hydrophobicity of the catalyst surface and that of the alcohol are also found to be decisive factors. The esterification activity of Al-MCF also compares favorably with that of ZSM-5, Al-SBA-15 and Al-MCM-41 catalyst, in particular when more bulky oleic acid was employed in the esterification reaction. Hence, the reaction is proposed to occur mainly within the pores of the catalyst. This observation indirectly proves planting of Brönsted acid sites insides the pores of the catalyst.

Acknowledgments The financial supports from the National Natural Science Foundation of China (20421303, 20473021, and 20633030), the National Basic Research Program of China (Grant No. 2003CB615807), the National High Technology Research and Development Program of China (2006AA03Z336), the Committee of the Shanghai Education (06SG03) and the Committee of Shanghai Science and Technology (07QH14003) are gratefully acknowledged.

References

1. Ogliaruso MA, Wolfe JF (1991) Synthesis of carboxylic acids esters and their derivatives. Wiley, New York
2. Haslam E (1980) Tetrahedron 36:2409
3. Koster R, van der Linden B, Poels E, Bliek A (2001) J Catal 204:333
4. Corma A, Garcia H, Iborra S, Primo J (1989) J Catal 120:78
5. Corma A (1997) Chem Rev 97:2373
6. Tuel Z (1995) Zeolites 15:236
7. Kloetstra KR, Van Bekkum H, Jansen JC (1999) Chem Comm 2281

8. Zhao D, Feng J, Huo Q, Melosh N, Fredrickson GH, Chmelka BF, Stucky GD (1998) Science 279:548
9. Schmidt-Winkel P Jr, Lukens WW, Zhao D, Yang P, Chmelka BF, Stucky GD (1999) J Am Chem Soc 121:254
10. Liu YM, Cao Y, Zhu KK, Yan SR, Dai WL, He HY, Fan KN (2002) Chem Commun 2832
11. Kutrowski P, Chmielarz L, Dziembaj R, Cool P, Vansant EF (2005) J Phys Chem B 109:11552
12. Schmidt-Winkel P Jr, Lukens WW, Yang P, Margolese DI, Lettow JS, Ying JY, Stucky GD (2000) Chem Mater 12:686
13. Zhang W, Shi J, Chen H, Hua Z, Yan D (2001) Chem Mater 13:648
14. Li Y, Zhang WH, Zhang L, Yang QH, Wei ZB, Li C (2004) J Phys Chem B 108:28
15. Borade RB, Clearfield A (1995) Catal Lett 31:267
16. Liu YM, Feng WL, Cao Y, Dai WL, He HY, Fan KN (2006) J Catal 239:125
17. Rabindran Jermy B, Pandurangan A (2005) Appl Catal A 288:253
18. Shanmugapriya K, Palanichamy M, Arabindoo B, Murugesan V (2004) J Catal 224:347
19. Griselda AM, Liliana BP, Gustavo AM, Oscar AA (2003) Catal Commun 4:118
20. Corma A, Fornes V, Navarro MT, Perez-Pariente J (1994) J Catal 148:569
21. Sakthivel A, Dapurkar SE, Gupta NM, Kulshreshtha SK, Selvam P (2003) Micro Meso Mater 65:177
22. Wang J, Huang L, Chen H, Li Q (1998) Catal Lett 55:157
23. Fan J, Yu CZ, Gao F, Lei J, Tian BZ, Wang LM, Luo Q, Tu B, Zhou WZ, Zhao DY (2003) Angew Chem Int Ed 42:3146